PROCEEDINGS, Thirty-Seventh Workshop on Geothermal Reservoir Engineering
Stanford University, Stanford, California, January 30 - February 1, 2012
SGP-TR-194

EXPERIMENTAL AND NUMERICAL EVALUATION OF CHANNELING FLOW IN FRACTURED TYPE OF GEOTHERMAL RESERVOIR

Takuya ISHIBASHI, Noriaki WATANABE, Nobuo Hirano, Atsushi OKAMOTO, and Noriyoshi TSUCHIYA

Tohoku University
6-6-20, Aramaki-aza-Aoba, Aoba-ku,
Sendai, Miyagi, 980-8579, Japan
e-mail: tishibashi@geo.kankyo.tohoku.ac.jp

ABSTRACT

In order to evaluate scale dependency in fracture flow under confining pressure, measurements of fracture surface topography at the atmospheric pressure and permeability at 30 MPa were conducted on granite samples containing different scaled fractures of 5 × 7.5 (37.5) cm^2, 10 × 15 (150) cm^2, and 20 × 30 (600) cm^2. Two kinds of fractures, mated and sheared fractures, were prepared for each scale. Moreover, fluid flows within aperture distributions of the fractures at the confining pressure were numerically determined using the data of fracture surface topography by matching numerical and experimental permeabilities. Based on the evaluation, scale-dependency was predicted as follows. Regardless of the fracture scale, the fluid flow is always characterized by channeling flow within an aperture distribution with a significant number of the contact points (zero-aperture) and a log-normal like distribution of the aperture. Since the surface roughness increases and the contact point does not change significantly with fracture scale, aperture for both mated and sheared fractures increases with fracture scale, where the relationship between the geometric mean of aperture and fracture scale (area or length of the fracture) is linear on log-log plot, with the slope of less than unity. The geometric standard deviation of aperture has no scale dependency. Despite of the scale dependency in aperture, permeability of mated fracture does not increase clearly with fracture scale, probably due to a small connectivity of the aperture. In contrast, permeability of sheared fracture increases with fracture scale, due to a large connectivity of the aperture that increases with fracture scale. Moreover, in case of a sheared fracture, the relationship between the permeability and fracture scale (area or length of the fracture) is linear on log-log plot, where the slope is less than unity.

INTRODUCTION

In fractured type of geothermal reservoirs, fracture networks are recognized as the predominant pathway of fluid. The discrete fracture network (DFN) model simulation, where a natural heterogeneity of the fracture network can be considered, has been one of the most effective ways to analyze fluid flow within fracture networks. In the DFN model simulation, fractures are, however, described by a pair of parallel smooth plates with a unique aperture [Jing et al., 2000; Tezuka et al., 2000] despite the fact that a real fracture has a heterogeneous aperture distribution due to the rough surfaces. Consequently, the conventional DFN model simulation neglects the formation of preferential flow paths (channeling flow) within the aperture distribution [Neretnieks, 2006; Watanabe et al., 2008, 2009, and 2010].

Therefore, in order to investigate channeling flow in a fracture network and its impacts on a development in a fractured type of geothermal reservoir, the authors developed a novel DFN model simulator, GeoFlow, in which fractures could have heterogeneous aperture distributions [Ishibashi et al., 2009]. The detail of GeoFlow simulator was described in APPENDIX. With using GeoFlow, we tried to conduct fluid flow simulation for a granite sample containing two intersecting fractures under confining pressure (Figure 1a). Note that the aperture distributions within the two fractures were determined using fracture surface geometry data. The GeoFlow simulation clearly exhibited 3-D channeling flow in the network of fractures (Figure 1b), which cannot be addressed with the conventional DFN model simulators. The present GeoFlow simulation provided a flow rate distribution in unidirectional flow, from top to bottom in the figure. Even visual observation revealed that the flow rate of Port 4 for Fracture B was dominant, which well corresponded to the most remarkable findings in fluid flow experiment with multiple-fracture sample (Figure 1a).

Thus, GeoFlow allows novel techniques for the investigation of 3-D channeling flow, especially in lab-scaled fracture network.

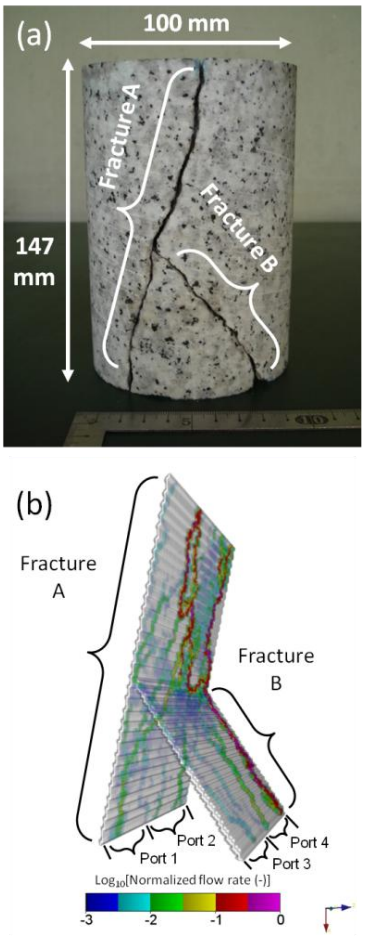

Figure 1: (a) Multiple-fracture sample containing two intersecting mated tensile fractures (Fracture A and B), and (b) the fluid flow model of the sample, as represented by a distribution of flow rate for the unidirectional fluid flow from top to bottom, as derived by the GeoFlow simulation.

However, the final goal in GeoFlow studies is the investigation of fluid flows in field-scale fracture networks. For this purpose, it is required to understand scale dependency in fracture flow under confining pressure. Although there were previous studies [Raven et al., 1985; Matsuki et al., 2006], the data on the scale dependency is limited and it is unclear how we should predict fluid flows within the heterogeneous aperture distributions of various sized fractures under confining pressure. The objectives of the present study are therefore to evaluate scale dependency in lab scale fracture flows under confining pressure in detail, and to discuss a method of the prediction based on the evaluations.

METHODS

In order to evaluate scale dependency in fracture flow under confining pressure, measurements of fracture surface topography at the atmospheric pressure and permeability at 30 MPa were conducted on granite samples containing different sized fractures. Moreover, fluid flows within aperture distributions of the fractures at the confining pressure were numerically determined based on the measured data.

Granite samples, which contained different sized single fractures of 5 × 7.5 (37.5) cm^2, 10 × 15 (150) cm^2, and 20 × 30 (600) cm^2, were prepared (Figure 2) by the following method. First, a tensile fracture was created in a cuboid of Inada granite (Ibaraki, Japan) using a wedge. The fractured granite was then fixed with mortar so that the fracture was either a mated or a sheared fracture. The sheared fracture was given a shear displacement of 5 mm in the direction of the sample radius. Finally, the fractured granite was cored and cut to the prescribed dimensions shown in Figure 2.

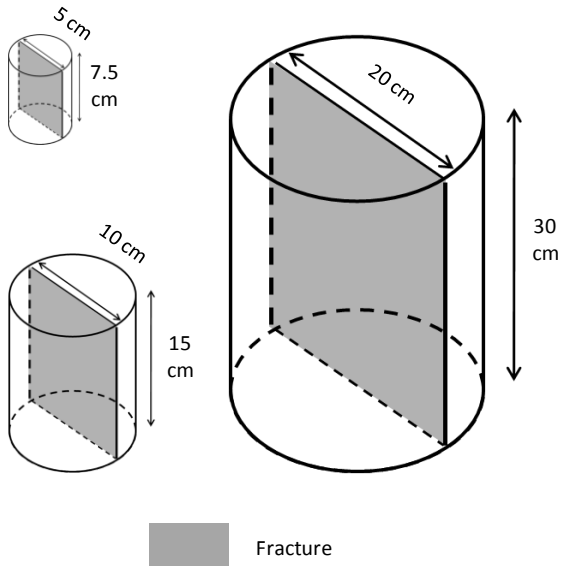

Figure 2: Granite samples containing the different sized single fractures.

A two dimensional (x-y) distribution of asperity height of the entire fracture plane was measured for all the fracture surfaces, in a 0.25-mm square grid system with Laser scanning equipment reported in Watanabe et al. [2008]. Moreover, in order to evaluate fracture surface roughness, the roughness coefficient (Z_2) and the tortuosity (τ), were calculated by [Sausse, 2002; Watanabe et al, 2009],

$$Z_2 = \sqrt{\frac{1}{N-1}\sum_{i=1}^{N-2}\left(\frac{z_{i+1}-z_i}{\Delta x}\right)^2}\ , \qquad (1)$$

$$\tau = \frac{\sum_{i=1}^{N-2}\sqrt{\left(z_{i+1}-z_i\right)^2+\left(\Delta x\right)^2}}{L}\ , \qquad (2)$$

where z_i is the asperity height, Δx is the distance between adjacent data points, L is the direct linear length, and N is the number of the data points, with respect to a two-dimensional (x-z or y-z) profile. The roughness coefficient is defined as the root mean square of local slopes, which provides a measure of microscopic (grid scale) roughness, whereas the tortuosity is defined as the ratio of the length of the profile line to the direct linear length, which provides a measure of macroscopic (sample scale) roughness.

After the measurement of fracture surface topography, unidirectional fluid (water) flow experiments along the sample axis were conducted on the samples at a confining pressure of 30 MPa. In these experiments, the flow rate through the sample and differential pressure between the ends of the sample were measured. Since the matrix permeability was low and a linear relationship between the flow rate and differential pressure was confirmed for all the samples, the fracture permeability (k) was calculated based on the cubic law assumption [Watanabe et al., 2008];

$$k = \frac{{e_h}^2}{12}\ , \qquad (3)$$

where e_h is the hydraulic aperture, which can be calculated from the following equation;

$$e_h = \left(-\frac{12\mu LQ}{W\Delta P}\right)^{1/3}, \qquad (4)$$

where Q is the flow rate, ΔP is the differential pressure, μ is the viscosity of water, and L and W are, respectively, the apparent lengths of the fracture in the directions parallel and perpendicular to the macroscopic flow direction.

Once data of the fracture surface topography at the atmospheric pressure and fracture permeability at a confining pressure are obtained for a fracture, a fluid flow within an aperture distribution of the fracture at the confining pressure can be determined by using the method reported in Watanabe et al. [2008].

The present fluid flow experiment can be simulated by the Reynolds equation for a steady-state laminar flow of a viscous, incompressible fluid within a two-dimensional (x-y) aperture distribution that can be created by the data of fracture surface topography [Brown, 1987; Ge, 1997; Sausse, 2002; Brush and Thomson, 2003; Matsuki et al., 2006; Nemoto et al., 2009; Watanabe et al. 2009];

$$\frac{\partial}{\partial x}\left(\frac{e^3}{12\mu}\frac{\partial P}{\partial x}\right)+\frac{\partial}{\partial y}\left(\frac{e^3}{12\mu}\frac{\partial P}{\partial y}\right)=0, \qquad (5)$$

where e is the local aperture, μ is the viscosity of water (constant value in the present study), and P is the fluid pressure. Since solution of Eq. (5) under the same boundary condition with that in the experiment provides numerical permeabilities, which can be compared with the experimental permeabilities, fluid flows within aperture distributions of the fractures at 30 MPa can be determined by matching numerical and experimental permeabilities through the fracture closing on a computer.

For the aperture distributions of the different sized fractures, contact area (percentages of the zero-aperture points, i.e. contact points, in the total data points), and a geometric mean and a standard deviation of the aperture (non-zero aperture) were evaluated. For the fluid flows (distributions of flow rate) within the aperture distributions, formations of preferential flow paths (channeling flows) were visualized.

RESULT

Figure 3 shows changes in the roughness coefficient and tortuosity with fracture size (area of the fracture in the present study). Both the roughness coefficient and tortuosity increased with fracture size.

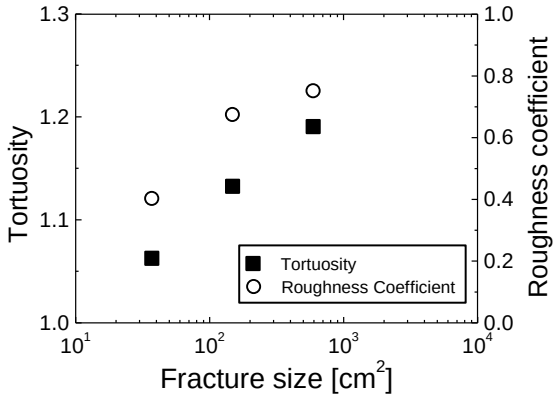

Figure 3: Changes in the roughness coefficient and tortuosity with fracture size.

Figure 4 shows changes in the permeability with fracture size for the mated and sheared fractures at 30 MPa. For the mated fracture, permeability increased with increasing in fracture size from 5 × 7.5 (37.5)

cm^2 to 10 × 15 (150) cm^2, and decreased with increasing in fracture size from 10 × 15 (150) cm^2 to 20 × 30 (600) cm^2. Consequently, relationship between the permeability and fracture size was unclear for the mated fracture. In contrast, for the sheared fracture, permeability appeared to linearly increase with fracture size on log-log plot. Moreover, calculating the slope of the linear relationship, the slope was less than unity (approximately 0.4).

Figure 5 shows fluid flows within aperture distributions of the different sized mated and sheared fractures at 30 MPa. Regardless of fracture size, the aperture distribution had a strong heterogeneity due to a significant number of contact points, which was represented as 1 μm-aperture in Figure 5, and a wide range of the aperture from micrometer to millimeter scale. As a result, for all the fractures, fluid flow occurred along preferential flow paths (i.e. channeling flow), which was represented as points having the flow rate greater than 1% of total flow rate in Figure 5. Moreover, tortuosity of the flow paths appeared to be greater for the mated fracture.

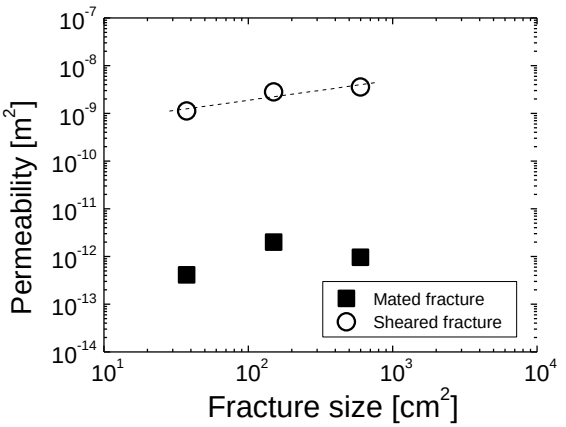

Figure 4: Changes in the permeability with fracture size for the mated and sheared fractures at 30 MPa.

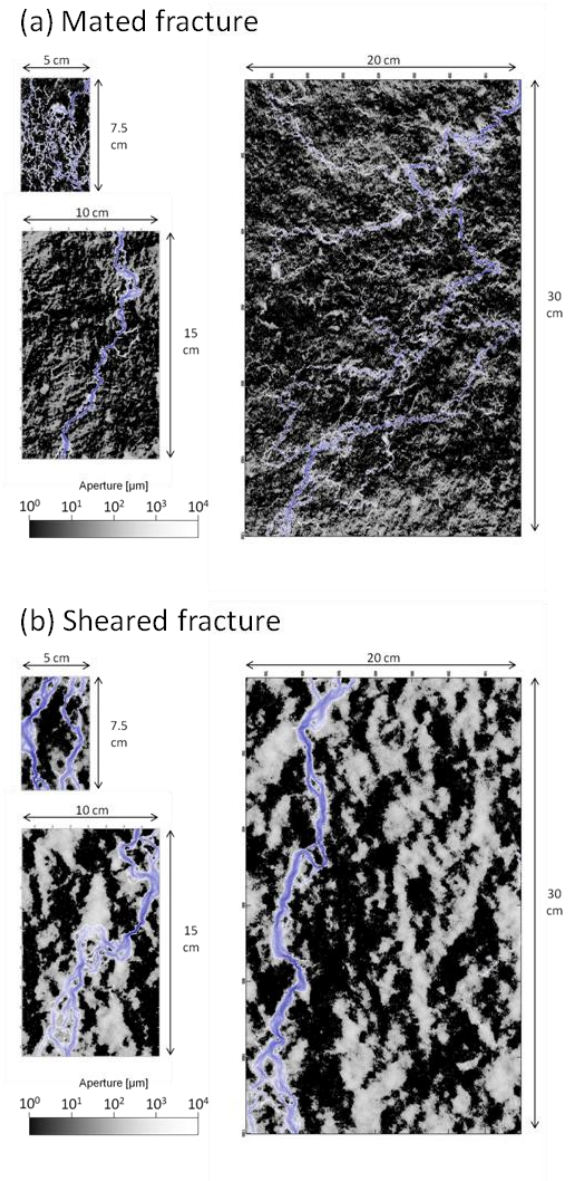

Figure 5: Fluid flows within the aperture distributions for the different sized mated (a) and sheared (b) fractures at 30 MPa.

As shown in Figure 6, histogram of the aperture was always characterized by a significant number of the contact points (i.e. contact area) and a skewed distribution of the (non-zero) aperture with long tail (i.e. lognormal-like distribution). Therefore, regardless of the fracture size, the contact area, the geometric mean and geometric standard deviation of the aperture were appropriate for characterization of the aperture distribution as reported in Watanabe et al. [2008 and 2009].

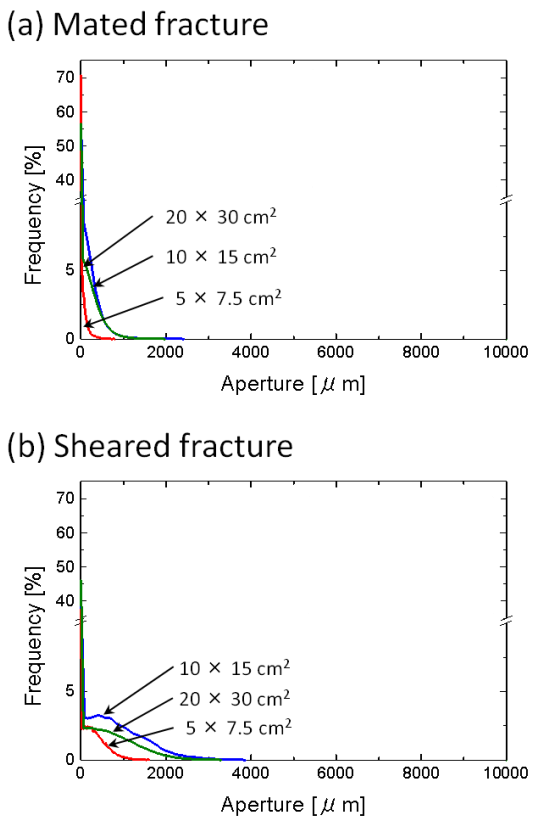

Figure 6: Histograms of the aperture for different sized mated (a) and sheared (b) fractures at 30 MPa.

Figure 7 shows changes in the contact area with fracture size for the mated and sheared fractures at 30 MPa. For the mated fractures, contact area significantly changed (decreased) only with increasing in the fracture size from 5 × 7.5 (37.5) cm^2 to 10 × 15 (150) cm^2, maybe due to a high degree of matedness of fracture surfaces for the smallest fracture. For the sheared fracture, the contact area appeared to increase with fracture size. However, the difference in contact area between the smallest and largest fractures was only 7%. Consequently, the scale dependency in contact area appeared to be insignificant for both mated and sheared fracture.

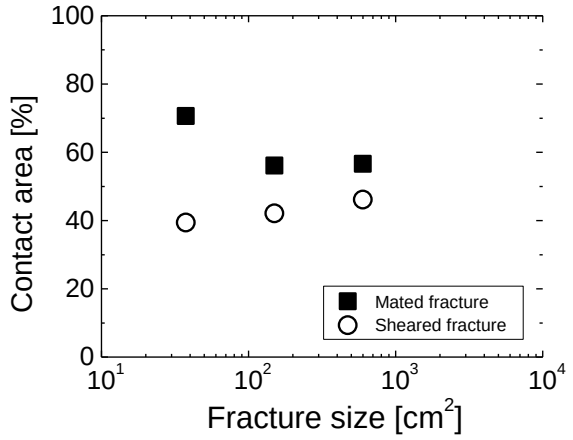

Figure 7: Changes in contact area with fracture size for mated fracture and sheared fracture at 30 MPa.

Figure 8 shows changes in the geometric mean of aperture with fracture size for the mated and sheared fractures at 30 MPa. The geometric mean of aperture appeared to linearly increase with fracture size on log-log plot for both mated and sheared fractures. Calculating the slope of linear relationships, the slopes were less than unity (approximately 0.4 and 0.3 for mated and sheared fractures, respectively), which was consistent with the field observation on a relationship between aperture and fracture length from centimeter to meter scales [Olson, 2003]. Although the fracture size is represented as area of the fracture in the figures of this paper, the linear relationship with the slope of less than unity can be confirmed even when using the length, instead of the area. On the other hands, the geometric standard deviation of aperture was almost constant (3.2 and 2.9 for mated and sheared fractures, respectively) throughout the fracture size.

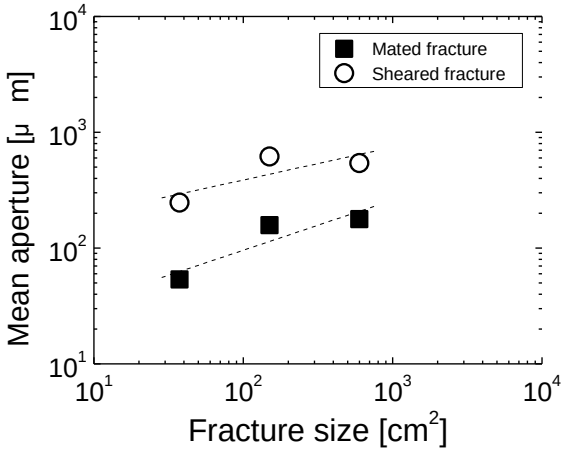

Figure 8: Changes in the geometric mean of aperture with fracture size for the mated and sheared fractures at 30 MPa.

DISCUSSIONS AND CONCLUSIONS

Based on the results described above, the scale dependency in aperture distribution of the fracture under confining pressure can be predicted as follows. Regardless of the fracture size, the aperture distribution always has a strong heterogeneity due to a wide range of the aperture and a significant number of the contact points (Figures 6 and 7). Since the surface roughness increases with fracture size (Figure 3) and the contact area has no significant scale dependency (Figure 7), the aperture increases with fracture size for both mated and sheared fractures. The geometric mean of aperture linearly increases with fracture size (area or length of the fracture) on log-log plot, where the slope of linear relationship is less than unity (Figure 8).

On the other hand, the scale dependency in fluid flow of the fracture under confining pressure can be predicted as follows. Regardless of the fracture size, the fluid flow is always characterized by the channeling flow (Figure 5). Probably due to a low connectivity of the aperture by the large contact area exceeding 50% (Figure 7), as inferred by the tortuous preferential flow paths (Figures 5), the permeability of the mated fracture does not show clear increase with fracture size (Figure 4), despite the clear scale dependency in aperture (Figure 8). In contrast, with increasing in fracture size, the permeability of sheared fracture increases which corresponds to the aperture increases (Figures 4 and 8), probably due to a high connectivity of the aperture by relatively small contact area (Figure 7), as inferred by less tourtuouity in the preferential flow paths (Figures 5). In addition, the permeability linearly increases with fracture size (area or length) on log-log plot, where the slope was less than unity.

The insignificant scale dependency in the contact area is a significant finding of importance, because this finding provides a method to predict fluid flows within aperture distributions in various scales through measurements of the surface topography and contact area for a lab scale fracture. Since fracture surfaces have the fractal nature [Power et al., 1997; Matsuki et al., 2006; Ogilvie et al., 2006], surfaces of various sized fractures can be predicted on a computer based on the measurement of the surface topography on a lab-scale fracture [Brown, 1995; Matsuki et al., 2006]. Consequently, aperture distributions of various sized fractures can be determined by closing a pair of numerical fracture surfaces to have the contact area of a lab scale fracture. This hypothesis will be examined in a future study, in order to investigate fluid flows within aperture distributions of much larger fractures.

APPENDIX: GEOFLOW SIMULATOR

We present here more detailed description of a novel discrete fracture network (DFN) model simulator, GeoFlow, for prediction of the 3-D channeling flow in a rock fracture network. In GeoFlow simulator, fractures are characterized by aperture distribution, rather than a unique aperture in the conventional DFN model simulator. A GeoFlow fluid flow simulation involves the following two main steps. A fracture network is first created in a 3-D analytic domain (*i.e.*, the matrix) by mapping 2-D fractures with aperture distributions. The Darcy flow through a matrix element interface is then calculated for an equivalent permeability continuum.

The fracture is a rectangular plane with dimensions of $L_i \times L_j$ in *i-j* coordinate system, while the analytic domain was a rectangular parallelepiped space with dimensions of $L_x \times L_y \times L_z$ in *x-y-z* coordinate system. The fracture is divided into $N_i \times N_j$ elements, where the fracture element is a rectangular cell with dimensions of $L_i/N_i \times L_j/N_j$, which has aperture value. The fracture is mapped in the *x-y-z* coordinate system by determining the coordinate of centroid and the direction of a specific pair of normal and tangent vectors for the fracture plane.

The analytic domain is divided into $N_x \times N_y \times N_z$ elements so that the matrix element is a rectangular parallelepiped cell with dimensions of $L_x/N_x \times L_y/N_y \times L_z/N_z$, followed by calculating a steady-state laminar flow of viscous and incompressible fluid for an equivalent permeability continuum. The Darcy's law based fluid flow model is described as;

$$\frac{\partial}{\partial x}\left(\frac{Ak}{\mu}\frac{\partial P}{\partial x}\right)+\frac{\partial}{\partial y}\left(\frac{Ak}{\mu}\frac{\partial P}{\partial y}\right)+\frac{\partial}{\partial z}\left(\frac{Ak}{\mu}\frac{\partial P}{\partial z}\right)=0, \tag{7}$$

where A is the cross-sectional area, k is the permeability, μ and P are the viscosity and pressure of fluid respectively. To determine Darcy flow through the matrix element interface, a finite difference form of Eq. (7) is solved under given boundary conditions, in which use of the product, Ak, represented by the following equation, characterizes the GeoFlow simulation:

$$Ak=\sum_n \frac{w_{f,n}\cdot a_{f,n}{}^3}{12}+A_m k_m , \tag{8}$$

where $w_{f,n}$ and $a_{f,n}$ are the width and aperture of nth fracture element intersecting the matrix element interface respectively, and A_m and k_m are the area and permeability of the matrix part respectively. The calculation for fracture element is based on the local

cubic law assumption [Ge, 1997; Oron and Brush and Thomson, 2003; Konzuk and Kueper, 2004]. Consequently, the permeability at the matrix element interface with fractures depends on both the fracture and the matrix permeabilities, whereas the permeability at the interface with no fracture depends only on the matrix permeability (Figure 9).

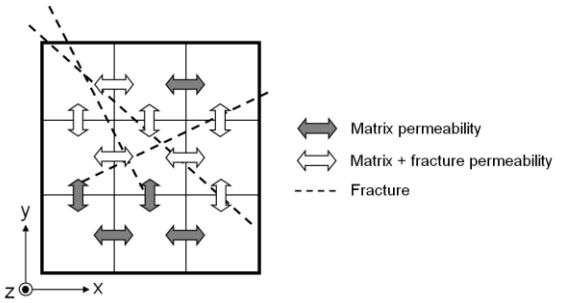

Figure 9: Conceptual diagram of permeability at the matrix element interface.

ACKNOWLEDGEMENT

The present study was supported in part by the Ministry of Education, Culture, Sports, Science and Technology (MEXT) through a Grant-in-Aid for Scientific Research on Innovative Areas, No. 22107502, the Japan Society for the Promotion of Science (JSPS) through a Grant-in-Aid for Young Scientists (A), No. 23686129, and the Japan Oil, Gas and Metals National Corporation (JOGMEC). The authors would like to thank Dr. Kimio Watanabe at Reneries, Ltd. for coding GeoFlow.

REFERENCES

Brown, S. R., 1987, Fluid flow through rock joints: The effect of surface roughness, *J. Geophys. Res., 92(B2),* 1337-1347.

Brown, S. R., 1995, Simple mathematical model of a rough fracture, *J. Geophys. Res., 100(B4),* 5941-5952.

Brown, S., A. Caprihan, and R. Hardly (1998), Experimental observation of fluid flow channels in a single fracture, *J. Geophys. Res., 103(B3),* 5125-5132.

Brush, D. J., and N. R. Thomson, 2003, Fluid flow in synthetic rough-walled fractures: Navier-Stokes, Stokes, and local cubic law assumptions, *Water Resour. Res., 39(4)*, 1085, doi:10.1029/2002WR001346.

Ge, S., 1997, A governing equation for fluid flow in rock fractures, *Water Resour. Res*., 33(1), 53-61.

Ishibashi, T., N. Watanabe, N. Hirano, A. Okamoto, and N. Tsuchiya, 2009, Development of discrete fracture network model simulator, GeoFlow, for evaluation of three dimensional channeling flow, paper IPTC 13143 presented at the 2009 International Petroleum Technology Conference, Doha (Qatar), Dec. 7-9.

Jing, Z., J.W. Richards, K. Watanabe, and T. Hashida, 2000, A three-dimensional stochastic rock mechanics model of engineered geothermal systems in fractured crystalline rock, *J. Geophys. Res., 105(B10),* 23663-23679.

Konzuk, J. S., and B. H. Kueper (2004), Evaluation of cubic law based models describing single-phase flow through a rough-walled fracture, *Water Resour. Res., 40*, W02402, doi:10.1029/2003WR002356.

Matsuki, K., Y. Chida, K. Sakaguchi, and P. W. J. Glover, 2006, Size effect on aperture and permeability of a fracture as estimated in large synthetic fractures, *Int. J. Rock Mech. Min. Sci.., 43(5)*, 726-755.

Nemoto, K., N. Watanabe, N. Hirano, and N. Tsuchiya, 2009, Direct measurement of contact area and stress dependence of anisotropic flow through rock fracture with heterogeneous aperture distribution, *Earth Planet. Sci. Lett., 281,* 81-87.

Neretnieks, I., 2006, Channeling with diffusion into stagnant water and into a matrix in series, *Water Resour. Res., 42,* W11418, doi:10.1029/2005WR004448.

Ogilvie, S. R., E. Isakov, and P. W.J. Glover, 2006, Fluid flow through rough fractures in rocks. Ⅱ: A new matching model for rough rock fractures, *Earth Planet. Sci. Lett., 241,* 454-465.

Olson, Joe E., 2003, Sublinear scaling of fracture aperture versus length: An exception or the rule?, *J. Geophys. Res., 108(B9),* 2413, doi:10.1029/2001JB000419.

Oron, A. P., and B. Berkowitz (1998), Flow in rock fractures: The local cubic law assumption reexamined, *Water Resour. Res., 34(11),* 2811-2825.

Power, W.L., and W.B. Durham, 1997, Topography of natural and artificial fractures in granitic rocks: Implications for studies of rock friction and fluid migration, *Int. J. Rock Mech. Min. Sci., 34(6),* 979-989.

Raven, K. G., and J. E. Gale, 1985, Water flow in natural rock fracture as a function of stress and sample size, *Int. J. Rock Mech. Min. Sci., 22(4),* 251-261.

Sausse, J., 2002, Hydromechanical properties and alteration of natural fracture surfaces in the Soultz granite (Bas-Rhin, France), *Tectonophysics, 348(1),* 169-185

Tezuka, K., and K. Watanabe, 2000, Fracture network modeling of Hijiroi hot dry reservoir by deterministic and stochastic crack network simulator (D/SK), *Proc. World Geotherm. Cong. 2000,* 3933-3983.

Watanabe, N., N. Hirano, and N. Tsuchiya, 2009, Diversity

of channeling flow in heterogeneous aperture distribution inferred from integrated experimental-numerical analysis on flow through shear fracture in granite, *J. Geophys. Res., 114,* B04208, doi:10,1029/2008JB005959.

Watanabe, N., N. Hirano, and N. Tsuchiya, 2008, Determination of aperture structure and fluid flow in a rock fracture by high-resolution numerical modeling on the basis of a flow-through experiment under confining pressure, *Water Resour. Res., 44,* W06412, doi:10.1029/2006WR005411.

Watanabe, N., T.Ishibashi, Y. Ohsaki, Y. Tsuchiya, T. Tamagawa, N. Hirano, H. Okabe, and N. Tsuchiya, 2010, Precise Three-dimensional Numerical Modeling of Fracture Flow Coupled with X-ray Computed Tomography for Reservoir Core Samples, *SPE Journal.*,SPE-146643-PA, doi:10.2118/146643-PA.